# Energetics of Intrinsic Defects in the Resistive Random Access Memory Material NiO

J. A. Dawson, Y. Guo and J. Robertson

*Department of Engineering, University of Cambridge, Cambridge CB2 1PZ, United Kingdom*

## ABSTRACT

Defect formation energies for a variety of intrinsic defects in the resistive random access memory (RRAM) material NiO are calculated and compared using *ab initio* methods in the form of screened exchange and the generalized gradient approximation (GGA) with Hubbard corrections. At the O-rich limit, Ni vacancies are the lowest cost defect for all Fermi energies within the gap, in agreement with the well-known *p*-type behaviour of NiO. At the Ni-rich (O-poor) limit, however, O vacancies dominate at lower Fermi energies. This chemical environment is considered the most likely in a RRAM context as the metal electrodes will shift the oxygen chemical potential towards the O-poor limit. Calculated band diagrams show that O vacancies in NiO are positively charged at the operating Fermi energy meaning that a scavenger metal layer is not required to maximise drift. Ni and O interstitials are generally found to be higher in energy than the respective vacancies suggesting that significant recombination of O vacancies and interstitials does not take place. The consequences of the band gap widening from the GGA + *U* method to the screened exchange functional for formation energies are also discussed.

*Electronic mail*: jad95@cam.ac.uk

## 1. Introduction

NiO is a technologically important material that finds use in a range of electronic and spintronic applications as a result of its interesting chemical and electronic properties. In recent years, one of the main focuses of NiO research has been the development of random access memories (RRAM) with the potential to challenge flash memory and become the next-generation of memory devices[1-3]. In addition to the typical advantages of transition metal oxide based RRAMs like easy fabrication and scalability, NiO has also shown low voltage and fast programming operations[2,4,5]. There is still debate over the physical origin and nature of the switching mechanism in RRAM devices and there is no exception for NiO-based RRAMs. Oxide-based RRAMs consist of an oxide layer between two electrodes with a thin metal layer adjacent to one of the electrodes so that oxygen can be scavenged from the oxide to form O vacancies[6]. The switching process begins via a forming step where the oxygen vacancies form into conductive path (filament) between the electrodes. However, other models involving metallic defects have been proposed to explain the formation of the filament[7-9]. It is therefore important to understand the fundamental atomic properties of NiO, so that we gain a deeper understanding into the critical processes in its application in memory devices. Recently, screened exchange calculations were used to study intrinsic defects in a selection of RRAM materials and the power of such computational techniques in determining the properties crucial for memory operation and the importance of understanding the defect processes in materials selection for memory devices were clearly illustrated.

There are several density functional theory (DFT) studies on intrinsic defects in bulk NiO[9-11], however, they only consider local-density methods (i.e. the generalized gradient approximation (GGA) and the local density approximation (LDA)) and the results are not entirely consistent with each other. These studies confirmed that vacancies are the most important and abundant defects in NiO and that Ni vacancies are indeed the main source of nonstoichometry in NiO, not O interstitials. All three works also agree that at Fermi energies ($E_F$) close to the valence band maximum (VBM) under metal-rich conditions, doubly charged O vacancies are the dominant defect with doubly charged Ni vacancies becoming increasingly more stable and dominant at higher $E_F$ values. Under O-rich conditions, Ni vacancies dominate the entire band gap, while the formation energy of O vacancies (hole killers) remains high resulting in low concentrations[10,12], thus satisfying the requirement for *p*-type behaviour. Disagreement between these studies arises from the value for the Ni vacancy defect formation energy. For formation of a neutral Ni vacancy at the VBM ($E_F = 0$), Lany *et al.*[10] and Yu *et al.*[11] report values of ~2.90 and 2.45 eV, respectively, whereas Lee *et al.*[9] suggest a significantly higher value of ~5.90 eV. It is unclear what produces this discrepancy, but perhaps it arises from different choices of atomic reference for Ni (and therefore different values of atomic chemical potential for Ni).

Local-density methods are subject to several serious shortcomings such as band gap underestimation, which is particularly large for NiO. While this error can be reduced using post-DFT methods like the inclusion of the Hubbard *U* parameter, it is not clear whether they are sufficiently accurate in predicting defect levels[13]. To correct this issue, we make use of screened exchange (sX) interactions and compare the results to those obtained from GGA + *U* calculations. Screened exchange has been successfully applied to a variety of materials and has been shown to give the correct band gaps of a wide range of semiconductors and insulators[13-16]. It is also capable of accurately describing the electronic structures of correlated systems like transition metal oxides including NiO[17]. The only previous study, to the best of our knowledge, to use a hybrid functional for defects in NiO was that of Ferrari and Pisani[18] who used the Becke hybrid-exchange functional with 20% exact exchange and the Perdew-Wang correlation functional (B3PW) to study cation and anion vacancies at the NiO (100) surface. In this work, we calculate defect formation energies and electrical energy levels for Ni and O vacancies/interstitials using the two different functionals in an attempt to further understand the key defect processes in NiO.

## 2. Method

Both the sX and GGA + *U* calculations were completed using the CASTEP plane-wave density functional theory code[19]. For the sX calculations, norm-conserving pseudopotentials for Ni and O were generated by the OPUIM method[20] and a plane-wave cutoff energy of 750 eV was used. For the GGA + *U* calculations, ultrasoft pseudopotentials were used along with the Perdew-Burke-Ernzerhof (PBE) functional[21]. Valence electrons in these calculations were described by a plane-wave basis set with an energy cutoff of 500 eV. A Hubbard correction of $U_{\text{eff}} = 5.3$ eV was used for the Ni 3*d* electrons. This value has proven to be successful in accurately reproducing the physical properties of NiO in numerous previous studies[9,18,21]. Defect calculations were completed using an antiferromagnetic ordered 128 atom 4 x 4 x 4 rhombohedral supercell. The internal geometry was relaxed within both sX and GGA + *U* using a single *k*-point placed at the Γ point and a 2 x 2 x 2 *k*-point mesh, respectively. Geometry optimizations were converged when forces became lower than 0.02 eV/Å.

The defect formation energy, $H_q$, as a function of Fermi energy ($\Delta E_F$) from the valence band edge ($E_V$) and the relative chemical potential ($\Delta\mu$) of element α, can be calculated from the total energies of the defective supercell ($E_q$) and the perfect supercell ($E_H$) using

$$H_q(E_F,\mu) = [E_q - E_H] + q(E_V + \Delta E_F) + \sum_\alpha n_\alpha(\mu_\alpha^0 + \Delta\mu_\alpha),$$

where $qE_V$ is the change in energy of the Fermi level when charge $q$ is added and $n_\alpha$ is the number of atoms of species α. The oxygen chemical potential ($\mu_O$) is attributed to that of the $O_2$ molecule, taken as zero, which is the O-rich limit. The Ni-rich (O-poor) limit corresponds to the Ni:NiO equilibrium and is equivalent to the experimental heat of formation of NiO (2.49 eV)[22].

## 3. Results and Discussion

The lattice parameter and band gap for NiO calculated using sX and GGA + *U* are given in Table 1, the experimental values are also provided for comparison. While the GGA + *U* lattice parameter suffers from the typical overestimation associated with the GGA functional, the sX value underestimates the lattice parameter, although it is still more accurate on comparison with the experimental value.

Table 1. Calculated and experimental lattice parameter and band gap for bulk NiO.

| | *a* (Å) | $E_g$ (eV) |
|---|---|---|
| sX | 4.11 | 3.85 |
| GGA + *U* | 4.26 | 2.50 |
| Experiment | 4.17[23] | 3.7-4.3[24,25] |

Fig. 1 shows the density of states (DOS) for NiO calculated using both the sX and GGA + *U* functionals. The VBM is set to 0 eV in both plots. The sX calculated band gap is far in excess of the GGA + *U* calculated value and is in much better agreement with experiment, although it should be noted that GGA + *U* itself is a significant improvement upon GGA which predicts insulating behaviour for NiO. The band gap of NiO arises from the combination of exchange splitting and additional crystal field splitting of the $e_g$ and $t_{2g}$ states and has been experimentally verified to be between 3.7 and 4.3 eV depending on the technique used[17,24,25]. Our band gap of 3.85 eV is also in good agreement with other hybrid functionals including the Heyd-Scuseria-Ernzerhof (HSE03) (4.1 eV)[26] and the Becke three-parameter Lee-Yang-Parr (B3LYP) (4.2 eV)[27]. It also agrees well with a value of 3.75 eV[28] calculated from one-shot self-energy correction calculations based on LDA + U wavefunctions at the GW level of approximation ($G_0W_0$@LDA + *U*). However, $G_0W_0$ with HSE03 wavefunctions and eigenvalues produces an overestimated band gap of 4.7 eV[26]. Our sX DOS and band gap are also in excellent agreement with previous sX calculations of NiO[17].

The valence band top of NiO is primarily made up of Ni 3d states with some O 2p states also present. This results in an unusually small electron affinity of 1.4 eV[29] which in turn means that the conduction band and valence band are located at 1.4 and ~5.4 eV below the vacuum layer, respectively. This is different to many other oxides (including those studied for RRAM applications (e.g. $HfO_2$, $TiO_2$, $Al_2O_3$ etc.)) where the valence band typically lies ~7-9 eV below the vacuum layer. This is an important point that we return to when discussing the

band diagrams for defective NiO. A more detailed discussion of the electronic structure and the performance of sX for NiO is available in REF. 17.

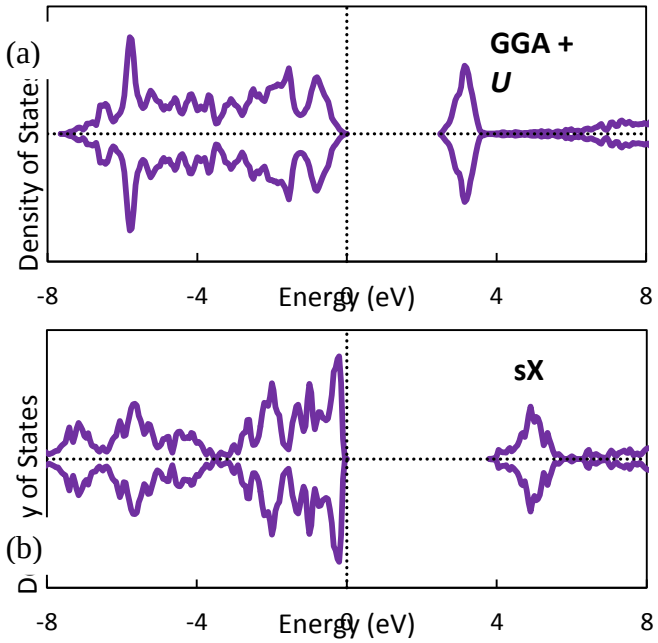


Fig. 1. DOS of NiO calculated using (a) GGA + *U* and (b) sX calculations.

The defect formation energies for intrinsic defects in NiO calculated using sX and GGA + *U* are plotted against $E_F$ in Fig. 2. We plot the energies for both the O-rich and Ni-rich limits and use Fermi energies of up to 4 eV in agreement with the experimentally determined NiO band gap. The appropriate environmental condition to consider is dependent upon the application and operating conditions. Typical preparation of NiO may take place under conditions closer to the O-rich limit, while for application in, for example, a water-cooled nuclear reactor, the conditions are considered to be close neither to the O-rich or O-poor limit[11,30]. For RRAMs, the metal electrodes or the scavenging metal shifts $\mu_O$ towards the O-poor limit and closer to $\mu_O$ of the scavenging metal/oxide equilibrium[6]. As discussed in a previous study[6], this means that $\mu_O$ is a key parameter in RRAM materials as the scavenging metal can be used to significantly lower it and therefore lower the formation energy of O vacancies or increase the formation energy of O interstitials, effectively controlling the defect concentrations. These are crucial points when considering defect energies in the context of RRAMs.

For the GGA + *U* calculations, Ni vacancies dominate under both conditions, in agreement with the observed Ni deficiency and *p*-type behaviour of NiO[31,32]. The results are also consistent with previous GGA + *U* calculations[9-11] which show that interstitials are generally unstable and that Ni vacancies are the lowest energy defects for the majority of $E_F$. O vacancies, however, do dominate at low values of $E_F$ at the Ni-rich (O-poor) limit. Widening of the band gap from GGA + *U* to sX has a significant effect on the defect formation energies. The formation energy of donor defects (i.e. positively charged O vacancies and Ni interstitials) at the VBM are reduced in energy, while the formation energies of the O interstitial and Ni vacancy have increased. Similar results[18] have also been reported for B3PW calculations of O and Ni vacancies at the NiO (001) surface, where a small reduction in the energy for an O vacancy (0.07 eV) and a large increase in the energy for a Ni vacancy (1.9 eV) was found when using the hybrid functional compared to GGA + *U*.

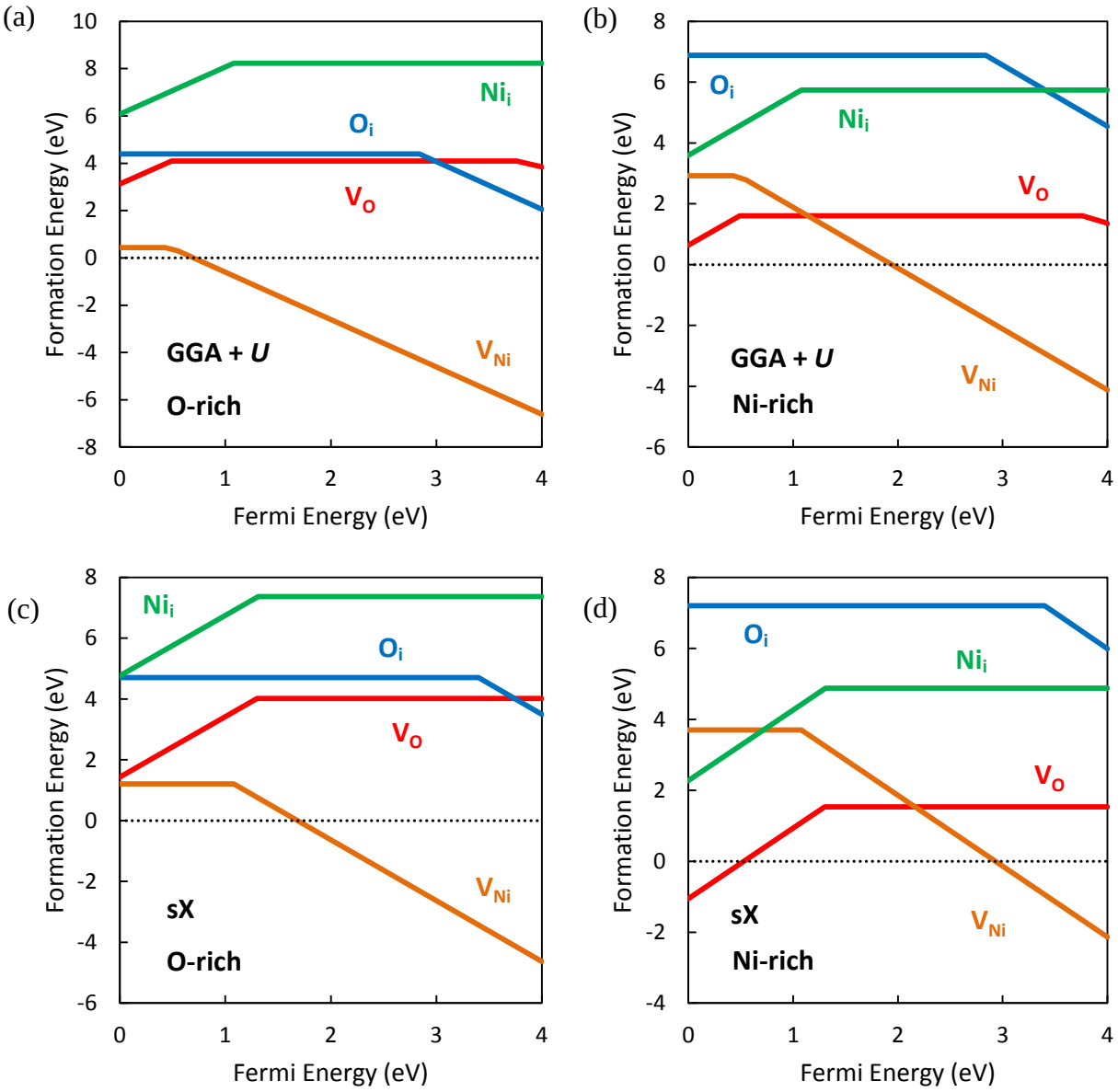


Fig. 2. Defect formation energies for NiO calculated using GGA + $U$ at (a) the O-rich limit and (b) the Ni-rich limit and sX at (c) the O-rich limit and (d) the Ni-rich limit.

This change in defect energies for the sX calculations now means that at the Ni-rich limit, O vacancies are the lowest energy defect for a larger range of $E_F$ than Ni vacancies. As this environmental condition is the most relevant for discussing RRAMs, it effectively means that the ability of the metal electrode to shift $\mu_O$ of the oxide causes NiO to behave in a way contradictory to its usual *p*-type nature. We do note, however, that the O vacancy formation energy is still larger than values calculated for $HfO_2$, $TiO_2$, $Ta_2O_5$ and $Al_2O_3$ using sX. Given that the formation energy of O interstitials is high in NiO, the energy for O Frenkel defects will also be high, in agreement with other RRAM oxides[6]. Therefore, we can rule out any significant recombination of O vacancies and interstitials in the RESET processes of RRAM as has been proposed in some mechanisms[33,34].

In order to assess the transition levels of the defects in NiO, we have produced band diagrams for each type of defect from the results of the two different functionals, these are

displayed in Fig. 3. The energies are aligned to the vacuum level and the Fermi level of the oxide's parent metal (Ni) is also plotted using its work function (-5.15 eV)[35]. As we have discussed, the unusually small electron affinity of NiO means that the VBM is not as deep as it is for other oxides. This fact in combination with the large metal work function of Ni means that the difference between the Fermi level and the VBM is very small (0.35 eV) and much smaller than the difference in other RRAM materials[6]. This means that the NiO/Ni combination is different from many other RRAM oxide/metal combinations in terms of defect level transitions, as we will discuss here.

At the Ni Fermi energy ($E_F$ = -5.15 eV), GGA + $U$ and sX predict the same charge states for each defect type. O vacancies and Ni interstitials are predicted to exist in their formal charge state (2+) at $E_F$. Alternatively, O interstitials and Ni vacancies are charge neutral defects at $E_F$. For the sX calculations, the defect charge transitions are simple with only one transition occurring either from 2+ to 0 or vice versa. For the GGA + $U$ calculations, the O vacancy undergoes a number of charge transitions, in agreement with previous computational studies[9,10]. The lowering of formation energy for donor defects using sX is reflected in the larger energy band for the charged O vacancy in Fig. 3(b).

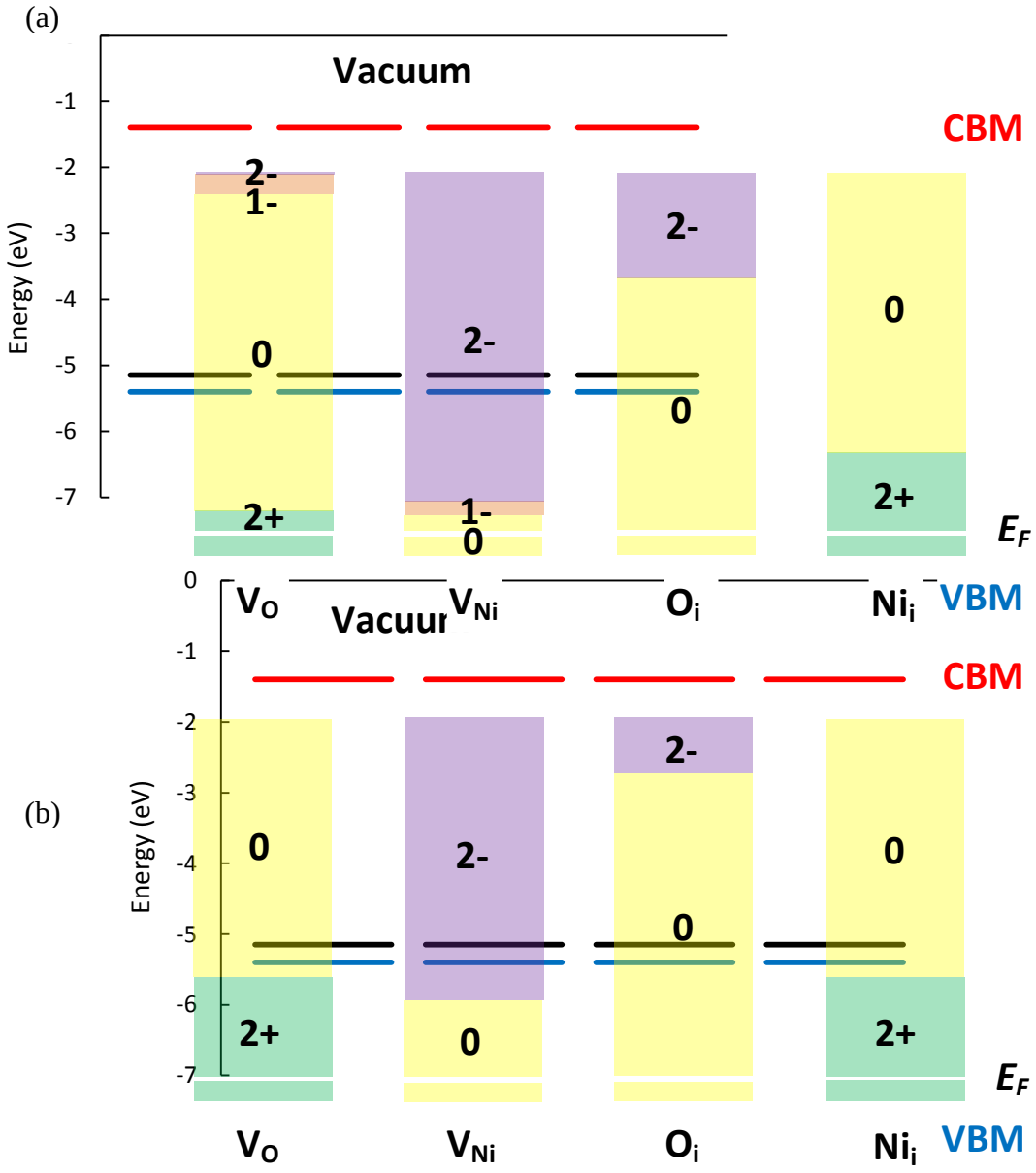

Fig. 3. Band diagrams for intrinsic defects in NiO calculated using (a) GGA + *U* and (b) sX. Energies are plotted with respect to the vacuum level and the Fermi level corresponds to the work function of Ni metal.

It is important for the O vacancy to be in a positive charge state at $E_F$, as this enables controlled drift under the switching field. However, this is not always the case when the parent metal of the oxide is used for the electrode, as has been shown for $HfO_2$, $Ta_2O_5$ and $Al_2O_3$ where O vacancies are neutral or even negatively charged[6]. For these oxide/metal setups, a less electropositive scavenging metal layer can be used to lower $E_F$ and therefore ensure positively charged O vacancies and potentially increase switching speed and endurance. For NiO, the unusually small energy difference between the VBM and $E_F$ ensures that O vacancies are positively charged at $E_F$ and that a scavenging metal is not required for this purpose. This is a distinct advantage for the use of NiO compared to some other RRAM materials. However, as discussed earlier, the concentration of O vacancies in NiO is unlikely to be as high as in other RRAM materials. In addition, the 0/2+ electrical transition energy for O vacancies in NiO occurs closer to the VBM, rather than closer to the CBM (conduction band minimum) as for other oxides[6], which means that the neutral O vacancy occupies a greater range of $E_F$ than the charged vacancy. These points are confirmed by both the GGA + *U* and sX calculations.

## 4. Conclusions

The energetics of intrinsic defects in the RRAM material NiO have been studied using first principle methods in the form of the GGA + *U* and sX functionals. We have calculated defect formation energies for O and Ni vacancies and O and Ni interstitials for a variety of charge states. We have also constructed band diagrams to analyse defect charge transition levels and find the defect charge states at the operating Fermi energy. Comparisons to other RRAM materials and comparisons between the two functionals are also made.

We have shown that at the O-rich limit, Ni vacancies dominate across the entirety of the Fermi level, in agreement with the well-known *p*-type behaviour of NiO. However, at the Ni-rich (O-poor) limit, the chemical environment considered most likely in a RRAM context as the metal electrodes will shift the oxygen chemical potential towards the O-poor limit, O vacancies dominate at lower Fermi energies, contrary to the usual behaviour of NiO. Band diagrams show that O vacancies in NiO are positively charged at the operating Fermi energy meaning that NiO has the advantage of not requiring a scavenger metal layer to maximise drift under the switching field.

**ACKNOWLEDGEMENTS**

**REFERENCES**

[1]S. Seo, M. J. Lee, D. H. Seo, E. J. Jeoung, D.-S. Suh, Y. S. Joung, I. K. Yoo, I. R. Hwang, S. H. Kim, I. S. Byun, J.-S. Kim, J. S. Choi, and B. H. Park, Appl. Phys. Lett. **85**, 5655 (2004).
[2]U. Russo, D. Ielmini, C. Cagli, and A. L. Lacaita, IEEE Trans. Electron Devices **56**, 186 (2009).
[3]H.-S. Philip Wong, H.-Y. Lee, S. Yu, Y.-S. Chen, Y. Wu, P.-S. Chen, B. Lee, F. T. Chen, and M.-J. Tsai, Proc. IEEE **100**, 1951 (2012).
[4]G. Baek, M. S. Lee, S. Seo, M. J. Lee, D. H. Seo, D.-S. Suh, J. C. Park, S. O. Park, H. S. Kim, I. K. Yoo, U.-I. Chung and I. T. Moon, in *Technical Digest IEDM* (2012), p. 587.

[5]K. Tsunoda, K. Kinoshita, H. Noshiro, Y. Yamazaki, T. Jizuka, Y. Ito, A. Takahashi, A. Okano, Y. Sato, T. Fukano, M. Aoki, and Y. Sugiyama, in *Technical Digest IEDM* (2007), p. 767.
[6]Y. Guo and J. Robertson, Appl. Phys. Lett. **105**, 223516 (2014).
[7]M. J. Lee, Y. Park, S. E. Ahn, B. S. Kang, C. B. Lee, K. H. Kim, W. X. Xianyu, I. K. Yoo, J. H. Lee, S. J. Chung, Y. H. Kim, C. S. Lee, K. N. Choi, and K. S. Chung, Appl. Phys. Lett. **103**, 013706 (2008).
[8]J. F. Gibbons and W. E. Beadle, Solid-State Electron. **7**, 785 (1964).
[9]H. D. Lee, B. Magyari-Köpe, and Y. Nishi, Phys. Rev. B **81**, 193202 (2010).
[10]S. Lany, J. Osorio-Guillén, and A. Zunger, Phys. Rev. B **75**, 241203 (2007).
[11]J. Yu, K. M. Rosso, and S. M. Bruemmer, J. Phys. Chem. C **116**, 1948 (2012).
[12]J. Osorio-Guillén, S. Lany, S. V. Barabash, and A. Zunger, Phys. Rev. Lett. **97**, 107203 (2006).
[13]S. J. Clark, J. Robertson, S. Lany, and A. Zunger, Phys. Rev. B **81**, 115311 (2010).
[14]S. J. Clark and J. Robertson, Phys. Rev. B **82**, 085208 (2010).
[15]S. J. Clark and J. Robertson, Phys. Status Solidi B **248**, 537 (2011).
[16]H.-Y. Lee, S. J. Clark, and J. Robertson, Phys. Rev. B **86**, 075209 (2012).
[17]R. Gillen and J. Robertson, J. Phys.: Condens. Matter **25**, 165502 (2013).
[18]A. M. Ferrari, C. Pisani, F. Cinquini, L. Giordano, and G. Pacchioni, J. Chem. Phys. **127**, 174711 (2007).
[19]M. D. Segall, P. J. D. Lindan, M. J. Probert, C. J. Pickard, P. J. Hasnip, S. J. Clark, and M. C. Payne, J. Phys.: Condens. Matter **14**, 2717 (2005).
[20]OPIUM pseudopotential package, http://opium.sourceforge.net.
[21]H. Chen and J. H. Harding, Phys. Rev. B **85**, 115127 (2012).
[22]B. J. Boyle, E. G. King, and K. C. Conway, J. Am. Chem. Soc. **76**, 3835 (1954).
[23]L. C. Bartel and B. Morosin, Phys. Rev. B **3**, 1039 (1971).
[24]Y. M. Ksendzov and I. A. Drabkin, Fiz. Tverd. Tela **7**, 1884 (1965).
[25]G. A. Sawatzky and J. W. Allen, Phys. Rev. Lett. **53**, 2339 (1984).
[26]C. Rödl, F. Fuchs, J. Furthmüller, and F. Bechstedt, Phys. Rev. B **79**, 235114 (2009).
[27]T. Bredow and A. R. Gerson, Phys. Rev. B **61**, 5194 (2000).
[28]H. Jiang, R. I. Gomez-Abal, P. Rinke, and M. Scheffler, Phys. Rev. B **82**, 045108 (2010).
[29]F. P. Koffyberg and F. A. Benko, J. Electrochem. Soc. **128**, 2476 (1981).
[30]J. G. Yu, R. Devanathan, and W. J. Weber, J. Phys.: Condens. Matter **21**, 43 (2009).
[31]J. Appel, Phys. Rev. **141**, 506 (1996).
[32]P. Kofstad, *Nonstoichiometry, Diffusion and Electrical Conductivity in Binary Metal Oxides* (Wiley Interscience, New York, 1972).
[33]N. Xu, B. Gao, L. F. Liu, B. Sun, X. Y. Liu, R. Q. Han, J. F. Kang, and B. Yu, in *VLSI Symp. Tech. Dig.* (2008), p. 100.
[34]B. Gao, S. Yu, N. Xu, L. F. Liu, B. Sun, X. Y. Liu, R. Q. Han, J. F. Kang, B. Yu, Y. Y. Wang, in *Tech. Dig. IEEE Int. Electron Devices Meeting*, (2008), p. 563.
[35]H. B. Michaelson, J. Appl. Phys. **48**, 4729 (1977).